Published in
Journal of Physics: Condensed Matter 21, issue 17, 174208 1-12, 2009
which should be used for any reference to this work

Photodetectors based on intersubband transitions using III-nitride superlattice structures

Daniel Hofstetter[1], Esther Baumann[1], Fabrizio R Giorgetta[1], Ricardo Théron[1], Hong Wu[2], William J Schaff[2], Jahan Dawlaty[2], Paul A George[2], Lester F Eastman[2], Farhan Rana[2], Prem K Kandaswamy[3], Sylvain Leconte[3] and Eva Monroy[3]

[1] University of Neuchatel, 1 A.-L. Breguet, 2000 Neuchatel, Switzerland
[2] Cornell University, Phillips Hall, Ithaca, NY 14853, USA
[3] Equipe mixte CEA-CNRS Nanophysique et Semiconducteurs, INAC/SP2M/PSC, CEA-Grenoble, 17 rue des Martyrs, 38054 Grenoble cedex 9, France

Abstract
We review our recent progress on the fabrication of near-infrared photodetectors based on intersubband transitions in AlN/GaN superlattice structures. Such devices were first demonstrated in 2003, and have since then seen a quite substantial development both in terms of detector responsivity and high speed operation. Nowadays, the most impressive results include characterization up to 3 GHz using a directly modulated semiconductor laser and up to 13.3 GHz using an ultra-short pulse solid state laser.

(Some figures in this article are in colour only in the electronic version)

1. Introduction

Intersubband transitions in semiconductor quantum wells (QWs) have a long and successful history. After first experimental evidence in transistor-like structures observed by Ando, Fowler, and Stern in 1982 [1], it was West and Eglash [2] who measured in 1985 the first intersubband absorption in a GaAs QW structure. The first practically useful devices were photoconductive detectors fabricated from GaAs/AlGaAs heterostructures by Levine [3] in 1987. Research in the following years was driven by an improvement of these photodetectors called quantum well infrared photodetectors (QWIPs) [4, 5], but also by a very intense activity towards the demonstration of a quantum cascade laser. This important step could be realized in 1994 by Faist *et al* at Bell Labs [6]. Research on quantum cascade lasers has without any doubt become the most impressive field of intersubband optoelectronics, with outstanding results in terms of continuous-wave operation of mid-infrared lasers above room temperature and expansion of semiconductor laser operation towards the terahertz spectral range [7–10].

At the other end of the electromagnetic spectrum, the extension of intersubband optoelectronics towards the near-infrared region is interesting for the development of ultra-fast photonic devices for optical telecommunication networks, as well as for application in a variety of chemical and biological sensors (pollution detection, chemical forensics, chemical and biological warfare, industrial process monitoring, medical diagnostics). Material systems with large enough conduction-band offsets to accommodate intersubband transitions at these relatively short wavelengths include InGaAs/AlAsSb [11], (CdS/ZnSe)/BeTe [12], GaInNAs/AlAs [13], and GaN/Al(Ga, In)N QWs [14–21]. In the case of III-nitride heterostructures, their conduction-band offset—around 1.8 eV for the GaN/AlN system [17, 20, 22–24]—is large enough to develop intersubband devices operating in the fiber-optics transmission windows at 1.3 and 1.55 μm. Additionally, thanks to their extremely strong electron-longitudinal optical phonon scattering effects, III-nitrides have the potential to outperform existing semiconductor-based telecommunication devices in terms of speed. That this statement is actually more than just a hypothesis, has been confirmed already by several experiments which demonstrated intersubband scattering times of the order of hundreds of femtoseconds [25, 26].

However, in comparison to the successful intersubband activities in the III-arsenide material system, the work on GaN and its alloys with AlN is still in its very early stage.

Experimental work on intersubband transitions using III-nitride alloys was initiated by C F Gmachl at Bell Laboratories in 1999. In a series of papers, she first demonstrated intersubband absorption at 'long' wavelengths ranging from 1.75 to 4.2 μm [27], followed by absorption down to 1.55 μm [14, 15]; later, she also gave first estimates for the ultra-short lifetime of excited electrons in AlN/GaN-based QWs [28, 29]. These early results impelled a number of activities in this interesting domain. For instance, Suzuki demonstrated passive optical switching in 2001 [30], Hofstetter showed intersubband absorption effects in the two-dimensional electron gas of a high electron mobility field effect transistor [31], and Julien succeeded in the first demonstration of intersubband absorption in a quantum dot structure [32]. Although the effort was quite considerable, it was not until 2003 that the first 'real' optoelectronic device, namely a photodetector, could be operated. This device, which was fabricated by Hofstetter [33], was a photovoltaic detector working up to 170 K and being most sensitive at 1.85 μm. However, its absorption characteristics were sufficiently broad to show an appreciable optical signal also at 1.55 μm. An additional boost for the III-nitride intersubband activity was provided by the European project NitWave, which reassembled the leading groups of Europe within the topic of intersubband transitions in III-nitrides. In the course of this project, many important achievements such as a low-loss waveguides [34], the first quantum dot infrared photodetector at 1.4 μm [35], the first photoconductive intersubband detector [36], the first intersubband intensity modulator [37–39], the first MOVPE-grown intersubband detectors [18, 40], the first photoconductive intersubband detectors using III-nitrides [41], the first III-nitride intersubband luminescence [42], 3 GHz operation of an intersubband photodetector [43–45], and high frequency modulation up to 10 GHz [46] were realized. At the same time, the Suzuki group performed a series of experiments aimed at a better understanding of the modulation properties of III-nitrides [47–49]. Additionally, there has been an important research effort on saturable absorbers for ultra-fast all-optical switching [48, 50–52]. GaN-based all-optical switches with an extinction ratio larger than 10 dB have been demonstrated recently [54, 55].

Although overall, substantial progress has been made in many respects, there are still dark areas which require additional research effort. As a representative example, it is still somewhat unclear how to optimize a simple QW detector structure in terms of operating speed or responsivity. In any case, one can say that the topic of intersubband transitions in III-nitrides remains a very interesting one, having a considerable potential for surprises. This is mainly a consequence of the (too) fast early success of violet-blue laser diodes, which prevented a large fraction of the III-nitride community doing their homework properly: namely to understand many of the fundamental effects of these fascinating materials. As a matter of fact, lots of basic material properties were initially masked by poor material quality. The classical example is the bandgap of InN which was believed to be 1.89 eV for more than 20 years [53] until high quality thin films grown at Cornell University by Hai Lu *et al* revealed a much lower value of 0.6 eV [54]. Defects, too high doping levels, and oxygen contamination of the films had led to the wrong conclusions published in 1977. The purpose of this paper is therefore going into two directions. First, the current status of III-nitride intersubband photodetectors—in particular those based on QW structures—will be reviewed. But second, we would also like to point out problems in order to stimulate further research effort and to improve the general knowledge of III-nitride semiconductors.

The paper will be organized as follows: in section 2, we present a short introduction to simulation tools and summarize the device parameters that provide a better description of our experimental results. In section 3, we then briefly address some important issues of material growth and device fabrication. In section 4, first material and device results are described, and the following fifth section is devoted to non-linearity measurements on our devices. Some more detector-specific high frequency measurements constitute the topic of section 6. Finally, two examples of differently designed intersubband detectors in the III-nitrides are presented in section 7. The paper concludes with a short summary and outlook.

2. Simulations and design

Simulation work in the III-nitride material system is an extremely challenging task because of the uncertainty in material parameters, the lattice mismatch between GaN and AlN, the relaxation particularities of wurtzite nitride materials which result in a final strain state that depends significantly on the growth conditions, and strong internal pyro- and piezoelectric polarization fields [55, 56]. One has to take into account that a standard GaN/AlN interface accommodates a fixed charge density that can be higher than 5×10^{13} cm^{-2} electrons. This huge charge density leads to an internal field in GaN/AlN nanostructures of the order of 5–10 MV cm^{-1}. In addition, the required QW thickness for intersubband effects at 1.55 μm is only 5–6 ML. Whether any standard calculation method such as the envelope function approach still renders valid results for such thin QWs is not *a priori* clear. Therefore, we will have to be very careful with the interpretation of any simulation in this material system. In the best case, the simulations can be used as design guidelines, but not as any kind of strict rules or valid confirmation of the absolute position of any energy levels.

Since our work concentrated mostly on the fabrication of QW-based devices, this paragraph will already be quite specific for this particular class of structures. All our band structure simulations were based on self-consistent Schrödinger–Poisson equation solvers. We worked with two different programs; the first one was an adapted version of 'cband', which is a program developed at Cornell University for band structure calculations on AlGaN/GaN-based high electron mobility transistors [57, 58], while the second is an adapted version of 'calculeband', a program developed by Sirtori and Faist mainly for the simulation of quantum cascade lasers [59], modified to include the effects of internal fields in III-nitrides on the bandstructure. 'Cband' has the advantage of taking into account more realistic boundary

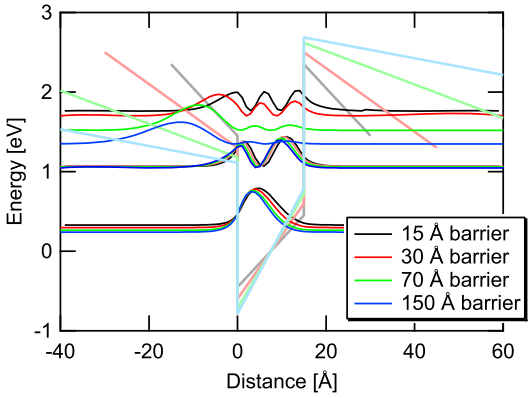

Figure 1. Simulated band structure for a constant GaN:Si QW thickness of 15 Å and four different AlN: intrinsic barrier thicknesses (15, 30, 70, and 150 Å).

conditions for the distribution of the charge carriers, leading to a better approximation of the band structure in terms of overall band deformations due to the internal piezo- and pyro-electric fields. On the other hand, 'calculeband' has certain advantages in terms of 'local exactness'; this is mainly due to a more sophisticated implementation of non-parabolicity effects. 'Calculeband' uses an effective two band model according to the theory paper of Sirtori and Faist [40]. It places the simulated band structure into a rectangularly shaped potential well in order to guarantee bound wave functions for all energy states. The potential is then discretized by small 'potential slices' and the Schrödinger equation is being solved piecewise using a transfer matrix method. The non-parabolicity is taken into account via an energy-dependent effective mass. In contrast, 'cband' is based entirely on matrix formalism and solves the Schrödinger equation in matrix form and self-consistently by direct diagonalization of the Hamiltonian. This results in better convergence for long superlattices, but in a slightly deteriorated description of the eigenenergies of single quantized states. Therefore 'cband' is especially useful if the overall band structure is looked for, whereas 'calculeband' has slight advantages if, for instance, the bound levels of a single or a double QW are needed.

In figure 1, we present a 'calculeband' simulation for a series of samples having a constant QW thickness of 1.5 nm and barrier thicknesses ranging from 1.5 to 15 nm. For the simulation, we assumed that the layers would be 100% strained onto the underlying AlN buffer layer. According to the theory presented in Ambacher *et al* [60], the internal pyro- and piezo-electric polarizations can be treated like this

$$P_{\mathrm{sp}}^{\mathrm{AlGaN}}(x) = -0.090x - 0.034(1-x) + 0.021x(1-x) \quad (1)$$

$$P_{\mathrm{piezo}}^{\mathrm{AlGaN/AlN}}(x) = 0.026(1-x) + 0.0248x(1-x) \quad (2)$$

$$P_{\mathrm{piezo}}^{\mathrm{AlGaN/GaN}}(x) = -0.0525x + 0.0282x(1-x) \quad (3)$$

where x is the Al concentration of the AlGaN compound, and $P_{\mathrm{sp}}^{\mathrm{AlGaN}}(x)$ is the pyro-electric polarization for AlGaN. Equation (1) describes the spontaneous polarization of AlGaN compounds, equation (2) stands for the piezo-electric polarization, $P_{\mathrm{piezo}}^{\mathrm{AlGaN/AlN}}(x)$, of an AlGaN layer grown fully strained on AlN, while equation (3) describes the piezo-electric polarization, $P_{\mathrm{piezo}}^{\mathrm{AlGaN/GaN}}(x)$, for an AlGaN layer on top of GaN. According to the work of Bernardini and Fiorentini [61], the internal fields F_{int} in the superlattice structure are related to the respective polarizations and layer thicknesses by

$$F_{\mathrm{int}}^{\mathrm{GaN}} = \frac{t_{\mathrm{AlN}}(|P_{\mathrm{sp}}^{\mathrm{GaN}}| - |P_{\mathrm{piezo}}^{\mathrm{GaN}}| - |P_{\mathrm{sp}}^{\mathrm{AlN}}| - |P_{\mathrm{piezo}}^{\mathrm{AlN}}|)}{\varepsilon_{\mathrm{AlN}} t_{\mathrm{GaN}} + \varepsilon_{\mathrm{GaN}} t_{\mathrm{AlN}}} \quad (4)$$

$$F_{\mathrm{int}}^{\mathrm{AlN}} = \frac{t_{\mathrm{GaN}}(|P_{\mathrm{sp}}^{\mathrm{AlN}}| + |P_{\mathrm{piezo}}^{\mathrm{AlN}}| - |P_{\mathrm{sp}}^{\mathrm{GaN}}| + |P_{\mathrm{piezo}}^{\mathrm{GaN}}|)}{\varepsilon_{\mathrm{AlN}} t_{\mathrm{GaN}} + \varepsilon_{\mathrm{GaN}} t_{\mathrm{AlN}}} \quad (5)$$

where $\varepsilon_{\mathrm{AlN}}$ and $\varepsilon_{\mathrm{GaN}}$ are the dielectric constants for AlN and GaN, respectively, while t_{AlN} and t_{GaN} are the corresponding layer thicknesses. Using (1)–(5) allows us then to calculate the internal polarization fields in a III-nitride superlattice. The values obtained using these formulae served as input parameters for the band structures in figure 1. Figure 2 shows a comparison of measured intersubband transition energies with those obtained in figure 1 using the simulation. Given the large number of involved parameters and their large uncertainty, the agreement is quite good. Keeping in mind that the piezo-electric polarization depends on the strain in the crystal, it is obvious that among the different samples, the changing amount of residual biaxial strain strongly influences the size of the piezo-electric field; this leads to a changing amount of quantum confined Stark effect. Extended bond x-ray

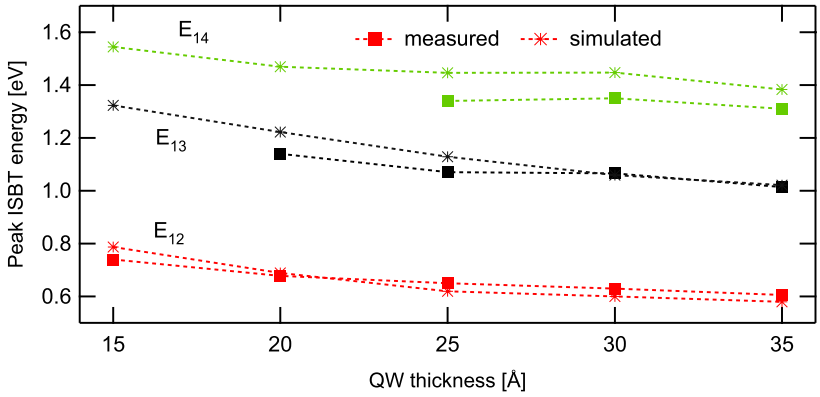

Figure 2. Comparison between simulated and experimentally determined intersubband transition energies in a series of QWs with thicknesses ranging from 15 to 35 Å.

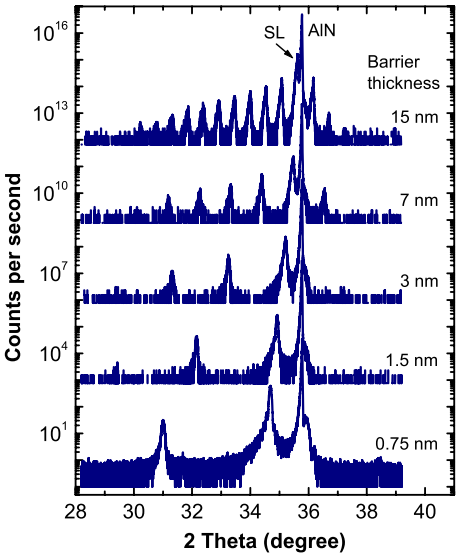

Figure 3. X-ray diffraction scans of five different samples with different superlattice periods (QW thickness 15 Å/barrier thicknesses of 7.5, 15, 30, 70, and 150 Å).

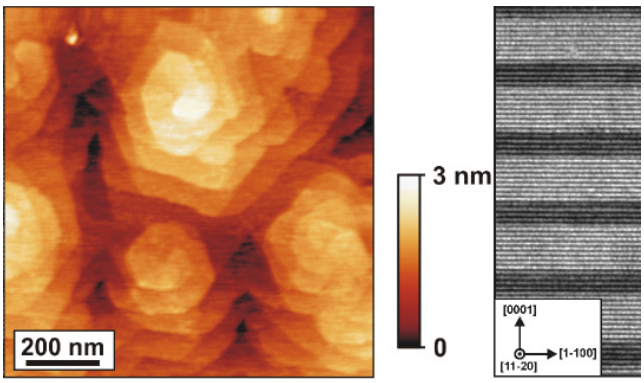

Figure 4. (a) Atomic force microscopy surface scan and (b) transmission electron microscopy image of a superlattice sample grown by PAMBE.

measurements have shown that even in a 10 period superlattice, the topmost layers will be no longer entirely strained on the AlN buffer layer. Although this particular feature of AlN/GaN-superlattices makes the predictive power of such simulations somewhat questionable, we were nevertheless able to confirm certain trends seen in the experiments below.

The typical band structure for an infrared QW detector using III-nitrides and operating at 1.55 μm consists of an insulating AlN buffer, on top of which a superlattice with usually 40 periods of 1.5 nm thick GaN:Si QWs and 1.5–15 nm thick non-intentionally doped AlN barrier layers is grown. The entire structure is capped with an insulating AlN layer of 50 nm thickness. Figure 3 shows a series of x-ray diffraction scans for such samples. According to the different periods of the five presented samples, we observe a different number of superlattice reflections. But even for a small period of 3.0 nm (1.5 nm QW/1.5 nm barrier), these reflections are visible up to the second order, which is a clear indication for the high structural quality of the grown material. The doping level is kept very high, on the order of 5×10^{19} cm^{-3}. According to a paper published by Monroy *et al* [62], and in contrast to earlier reports [63], no detrimental effects of the high Si doping level on the crystalline quality could be observed. As a beneficial side effect, heavy doping allows also a straight-forward characterization of the intersubband absorption in a multi-pass absorption experiment. Besides the barrier thickness and the doping level, all other relevant device parameters such as number of periods, QW thickness, or cap layer thickness have been varied systematically in search for optimized performance. We will present some of the results of these studies in the section about characterization. At this point, it is nearly impossible to justify the particular choice of all layer thicknesses and doping levels in an analytic way. Obviously, the QW thickness has the most directly measurable influence on the absorption wavelength, but other parameters such as cap layer thickness, barrier thickness, or number of periods have—at least in the beginning of this work—been chosen somewhat arbitrarily.

3. Crystal growth and fabrication

GaN/AlN QW structures can be grown either by molecular beam epitaxy (MBE) or by metal–organic vapor phase epitaxy (MOVPE). Most of the results to be presented here are based on material grown by plasma-assisted MBE (PAMBE). The lower growth temperature of this technique results in sharp GaN/AlN interfaces, which is a critical requirement to achieve device operation at 1.55 μm. Details about the growth procedure can be found in the work of Monroy [64, 65]. For completeness sake, we give nevertheless some general information concerning the growth procedure. All PAMBE samples are grown on AlN-on-sapphire growth templates fabricated by MOVPE. The AlN layer has a thickness of roughly 1 μm and the orientation of the substrate is C-face. During the growth of the PAMBE layers, different methods have been investigated in order to guarantee metal-rich growth conditions, which in turn result in smooth surfaces. More particularly, In used as a surfactant, Ga excess, and growth interruptions along with Ga and Al excess for GaN and AlN layers, respectively, have been tried out. From a morphological point of view, the three different methods gave comparable results, however, the crystalline quality of the Ga excess samples was highest, so that most layers of the present paper were grown using this method. A typical characterization of sample morphology and interface quality using atomic force microscopy (AFM) and transmission electron microscopy (TEM) is presented in figures 4(a) and (b), respectively. The AFM analysis showed a root-mean-square (rms) surface roughness which remained around 0.6 nm in an area of 2.5 $\times$ 2.5 μm^2. From the analysis of the TEM picture, we conclude that the GaN/AlN interfaces are abrupt at the monolayer scale.

As far as the fabrication process is concerned, most devices presented here went through a very straight-forward fabrication procedure. For simplicity reasons, absorption and photovoltage samples were usually processed in exactly the same way. Using diamond-containing polishing films, we

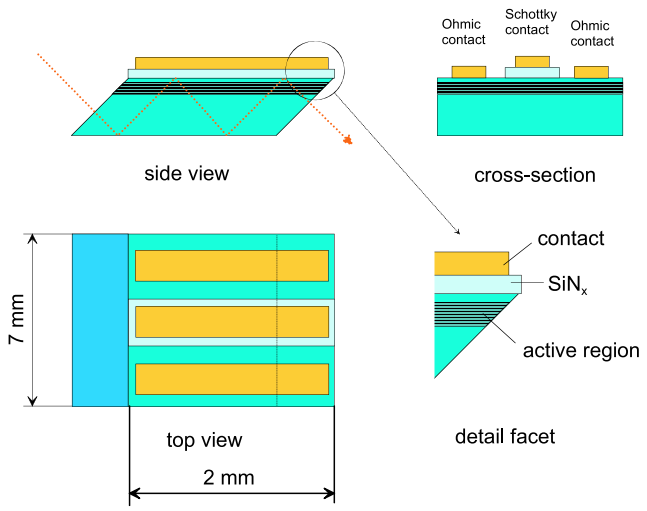

Figure 5. Schematic representation of the sample's geometrical dimensions including the metal stripes used for contacting.

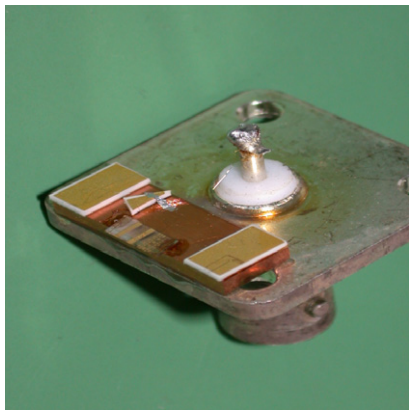

Figure 6. Photograph of a photodetector sample used in a high frequency experiment. The BNC connector is clearly visible.

polished first the back of the wafer (1 μm grit size), and then two parallel, 45° inclined facet mirrors in order to facilitate optical coupling into the wafer. As schematically shown in figure 5, the typical dimensions of such a sample are 2 mm between the two parallel wedged facets and 7 mm in length (dimensions in figure 5 are not to scale!). We then thermally evaporated three metal stripes (Ti/Au, 10/500 nm, unannealed) running from wedge to wedge and having a dimension of roughly 0.5 × 2 mm^2. The central stripe was evaporated on a thin Si_3N_4 layer in order to form a Schottky contact. Measurements could be done either by connection of an ohmic–ohmic or an ohmic–Schottky contact pair. Mounting on a copper heatsink and wire bonding of the two contacts to Au-coated ceramic platelets completed the process. A photovoltage can then be measured between the illuminated signal and the dark reference contact of the sample. In the case of high frequency measurements, both fabrication method and mounting technique were slightly more sophisticated. The process involved evaporation of 100 × 100 μm^2 small metal contacts (Ti/Au, 10/500 nm). As figure 6 shows, mounting was then done directly on top of a BNC connector with a short bond wire going to the central pin of the connector and another one connecting to the ground contact of the connector to reduce the parasitic capacitance and inductance. It is obvious that this quite crude mounting technology suffers from parasitic effects which severely limit the high frequency behavior of our devices. We therefore expect that proper high frequency mounting using a coplanar strip-line, no wire bonds, and correct impedance matching will lead to marked performance improvements ($f_{3\ \mathrm{dB}} \approx$ 50–100 GHz) in terms of high frequency behavior.

4. Characterization

The main characterization tool for the presented work was a Fourier transform infrared (FTIR) spectrometer (Bruker IFS-66). The samples were mounted on the cold finger of a liquid He-flow cryostat, allowing measurements down to temperatures of 4.2 K. An external parabolic mirror setup focused the internal white light source of the FTIR onto the sample. For absorption measurements, the light passed through the device in a zig-zag mode and was analyzed via a broadband mercury–cadmium–telluride detector. For photodetector characterization, devices were connected to a Stanford Research current amplifier (SR570) whose output fed the external detector port of the FTIR. Figure 7 shows the results of a normalized transmission measurement taken on five different samples. The quantum confinement shift pushes the main absorption peak from 4800 cm^{-1} for a 35 Å QW towards 6000 cm^{-1} for a 15 Å QW. It is obvious that the absolute linewidth increases only slightly from 700 cm^{-1} for the thickest QW to about 800 cm^{-1} for the thinnest QW. Accordingly, the relative linewidth stays roughly constant at 13–15%. From these numbers, it is possible to estimate the level of interfacial roughness present in these samples; a conservative estimate results in roughly one monolayer on each interface. This number agrees well with the TEM picture analysis shown in figure 4(b). As usually observed with optical intersubband transitions, the quantum-mechanical polarization selection rule dictates that absorption be present in transverse magnetic (TM) polarization only.

In very general terms, the absorbance α of any intersubband transition can be described by the following formula

$$\alpha = \frac{4\pi q^2}{\varepsilon_0 n \lambda} \frac{\cos^2\theta}{\sin\theta} |\langle \varphi_1(z)|z|\varphi_2(z)\rangle|^2 n_s n_{\mathrm{pass}} n_{\mathrm{QW}} \qquad (6)$$

where q is the elementary charge, ε_0 the dielectric constant, n the refractive index, λ the center wavelength of the absorption peak, θ the angle of incidence from the surface normal, z the coordinate in the growth direction, $\varphi_1(z)$ and $\varphi_2(z)$ the envelopes of the ground- and the excited state wavefunctions, n_s the sheet carrier density, n_{pass} the number of passes through the QW region, and finally, n_{QW} the number of active QWs. As can be verified by equation (6), the absorption strength decreases with decreasing QW thickness: this is the result of the smaller dipole matrix element $d_{12} = \langle \varphi_1(z)|z|\varphi_2(z)\rangle$ in

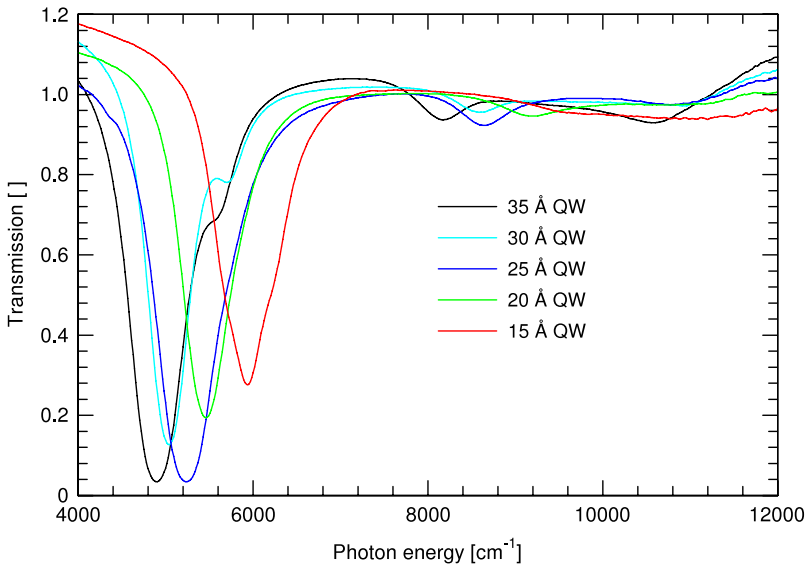

Figure 7. Absorption spectra of a series of five samples having different QW thicknesses (15, 20, 25, 30, and 35 Å) and showing the quantum confinement shift.

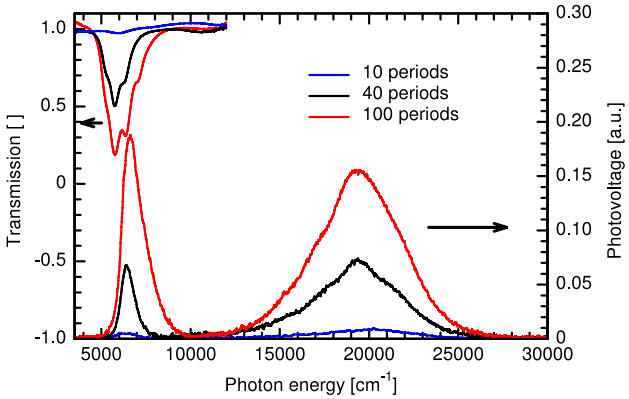

Figure 8. Absorption spectra of a series of samples with different number of active region periods (10, 40, and 100 periods).

smaller QWs. In larger (30 and 35 Å) QWs, we observed—in addition to the expected intersubband absorption signal—an absorption feature around 5500 cm^{-1}. The origin of this latter peak is not entirely clear yet. In any case, it cannot be due to a higher order intersubband transition such as the $E_1 \rightarrow E_3$ transition. Our calculations have indicated that this transition occurs at energies ranging from 8000 to 11 000 cm^{-1}. In addition, the existence of such higher order absorption peaks at the computed energies was verified experimentally; they are visible in figure 7 as small bumps. For the time being, the most probable explanation for the peaks around 5500 cm^{-1} is an impurity or defect level which provides additional states for the electrons to be absorbed into.

As mentioned earlier, we have varied several important design parameters—such as barrier thickness and number of periods—in a systematic way. Examples for the resulting measurements are shown in figures 8 and 9. Figure 8 shows the absorption and *relative* photovoltage for a series where the number of periods was varied from 10 via 40 to 100. In principle, it would be possible to put absolute values for the size of the photovoltage. However, for the following discussions, only the relative size of the photovoltage matters. We therefore use absolute units only in those cases where they are strictly necessary. This measurement series shows several interesting effects such as asymmetric linewidth broadening revealing a more and more pronounced high energy tail at increasing number of periods. This effect is clearly visible both in absorption and in photovoltage. The tail could be an indication of an increasing strain relaxation with increasing number of periods. As mentioned above in the paragraph on simulation, the changing amount of strain in the structure would in this case lead to a changing amount of Stark shift. As a second possibility, monolayer fluctuations as suggested by Tchernycheva [66] could also contribute to such an asymmetric broadening of the detection peak. The measurements show also a pretty good agreement between the expected and the experimentally observed relative signal strengths. Finally, an additional unpolarized photovoltaic signal centered at 20 000 cm^{-1} can be seen. We attribute this signal to defect levels corresponding to the yellow defect band in GaN from which electrons are being excited into the conduction band and swept towards the metal contacts by the Schottky junction underneath the non-annealed metal contacts.

Figure 9 shows the absorption measurements of a series of GaN/AlN QWs where the AlN barrier thickness was varied from 7.5 to 150 Å, and figure 10, presents the evolution of photovoltage signals as a function of temperature in the same sample series. This latter graph reveals clearly that thicker barrier layers result in a stronger photodetector signal than thin ones. A likely explanation for this phenomenon is a reduction in leakage current between single periods of the superlattice, leading to higher photovoltages. At 150 and 300 K, the sample with the thickest AlN barrier layer constitutes the best photodetector of the series. This experiment led us to the important conclusion that an optically non-linear effect rather

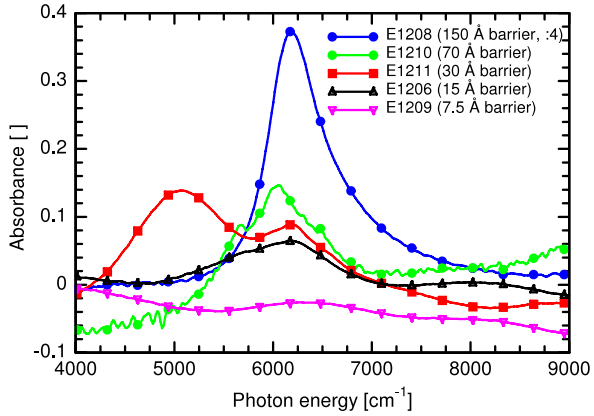

Figure 9. Series of samples with different AlN barrier layer thicknesses (7.5, 15, 30, 70, and 150 Å). Absorbance curves are shown.

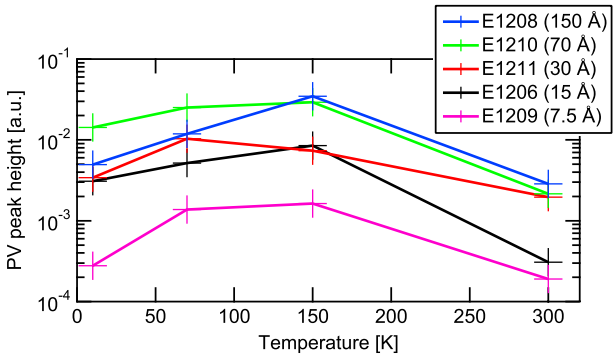

Figure 10. Photovoltage signal strength of the series of samples having different AlN barrier layer thicknesses as a function of temperature. The same sample series as in figure 9 was used.

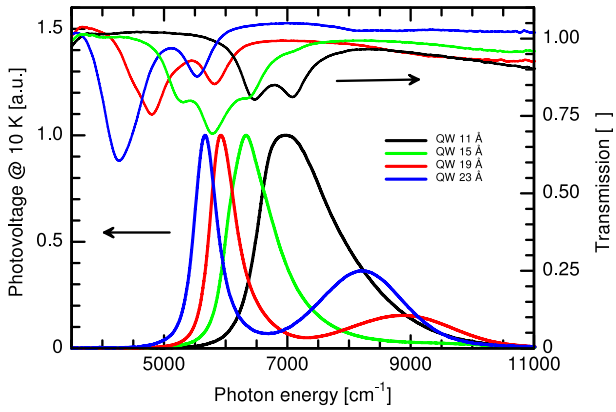

Figure 11. Photovoltage spectra of a series of four samples having different QW thicknesses (11, 15, 19, and 23 Å).

than a transport phenomenon, namely optical rectification, is at the origin of the observed intersubband photo-signal [67]. The functioning of these AlN/GaN-based devices can thus be explained via a small electron displacement in the growth direction which occurs thanks to the internal field-induced asymmetry of the QWs [68]. Since at the same time, the donor atoms do not move, small dipole moments will be

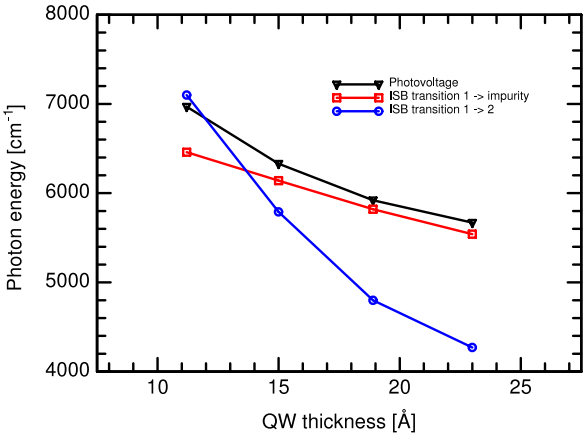

Figure 12. Energetic peak positions of absorption and photovoltage for the series shown in figure 11. A clear mismatch between absorption and photo-signal is visible, especially for thick QWs.

produced for each displaced electron. The sum of all dipole moments gets larger if the dwell time or the displacement of the electrons is increased. If ultra-high frequency operation is sought, one therefore has to find a trade-off between the dwell time and the desired frequency limit. This mechanism takes place only underneath the illuminated contact while the dark contact serves as a reference. An interesting question concerns the role of the two-dimensional electron gas being present at the superlattice-cap layer interface. One could imagine that the illumination-induced polarization of the superlattice would act like an additional pyro- or piezo-electric field. This could lead to an amplification of the observed photovoltage.

Figure 12 shows the evolution of the absorption and photovoltage signals taken from figure 11 as a function of QW thickness. It becomes obvious that an anticrossing occurs between the transition from level 1 into an impurity level and the regular intersubband transition from level 1 to level 2. This happens at roughly 13 Å QW thickness and manifests itself as strongly broadened absorption peak (see figure 11). Fortunately, nothing dramatic happens to the photovoltage signals at this energy: they neither show any additional broadening nor unexpected energetic shifts.

We have also made several temperature scans in order to better understand the behavior and the influence of thermal activation on our devices. Figure 13 shows the results of such scans for the sample series from figure 11 with different QW thickness: it is obvious that all detectors reach their responsivity maximum between 50 and 120 K. In addition, they all show a very steep signal decrease above about 200 K. A rapid change in the lateral conductivity of the AlN cap layer above 200 K could be responsible for this effect. This hypothesis was confirmed by I–V-characteristics as a function of temperature: the curves turn from more Schottky-like to Ohmic-like at about 220 K, indicating a new, more efficient leakage current path.

5. Non-linear effects

Our band structure simulations have shown that certain QW thicknesses can result in a configuration where the $E_1 \rightarrow$

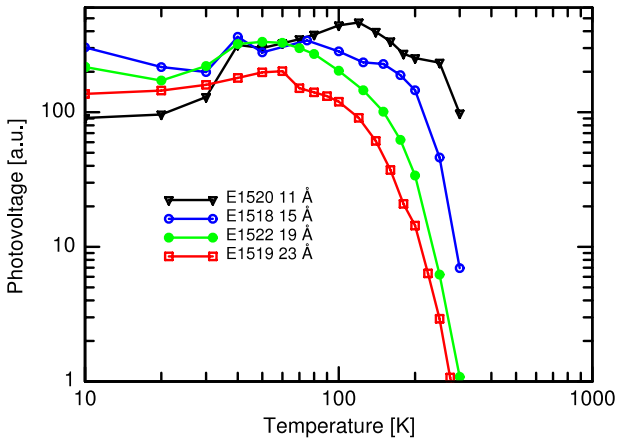

Figure 13. Responsivity of four detectors having different QW thicknesses as a function of device temperature. The steep slope at 200 K is clearly visible in every device. This is the same sample series as in figure 11.

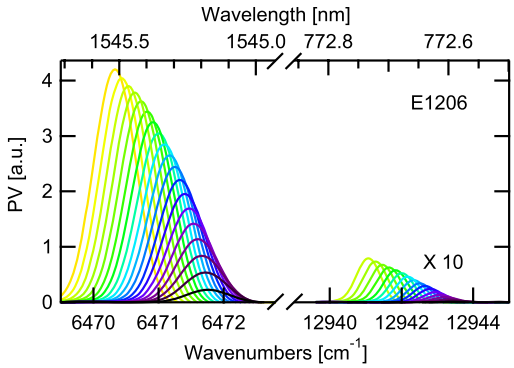

Figure 14. Series of detector signals as a function of laser injection current. A signal at the double frequency indicates an optical non-linearity.

E_2 transition has the same energy as the $E_2 \rightarrow E_3$ (or for very thick barrier layers the $E_2 \rightarrow E_4$) transition. This is an interesting experimental situation because it can result in the observation of third order non-linear effects such as two-photon absorption or saturation of the photovoltage signal under illumination with a strong laser beam. Indeed both effects have been observed experimentally, and we will describe them briefly in this paragraph.

Figure 14 shows a series of measurements performed under illumination with a commercial 1.55 μm laser diode. The laser current was increased linearly in steps of 5 mA up to a maximum of 100 mA. One can easily see that two detection peaks seem to be present in this case: one at 1.55 μm and another one at half this wavelength, namely at 775 nm. The fact of seeing these two peaks instead of only one has to do with our measurement setup which is based on a Fourier spectrometer. Any non-linearity in the detection leads to a distortion of the measured interferogram, and will thus automatically infer peaks at higher harmonic frequencies. As shown in figure 15(a), the intensity of the second harmonic peak grows quadratically with the intensity of the first harmonic peak. A further interesting fact in

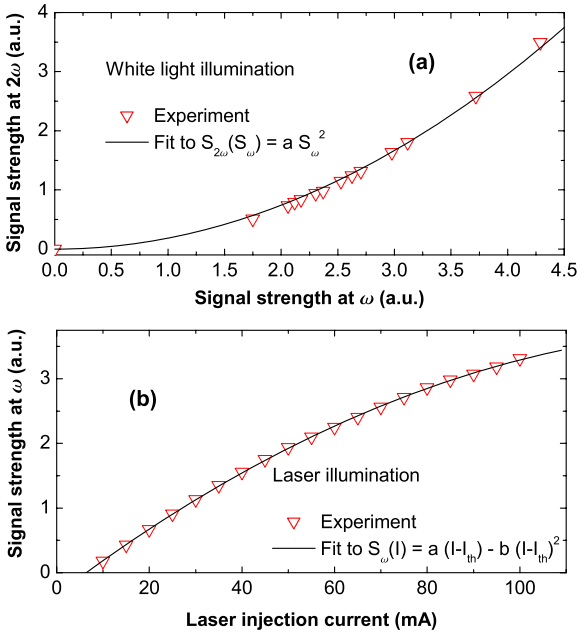

Figure 15. (a) Quadratic behavior of the second harmonic peak intensity as a function of the first harmonic peak. (b) Perfect fit of the measured data points using a sublinear quadratic saturation function as expected in our experimental configuration.

this experiment is given by the exactly quadratic saturation behavior of the detector signal at 1550 nm as a function of laser current and laser intensity. We performed a fit which yields a perfect matching of all experimentally observed data points, as reported in figure 15(b). This saturation effect is caused by the interplay between the three bound QW states which are in resonance with each other. Figure 16 shows schematically how the different energy levels are aligned within the QW and where the centers of gravity of the relevant wavefunctions are located. The latter point is crucial for the understanding of the non-linear effects in these detectors. If level E_2 loses electrons into level E_3, then the total non-linear dipole between levels E_2 and E_3 gets smaller. At the same time, when taking the center of gravity of level E_1 as a reference, the center of gravity of level E_3 is shifted towards negative values whereas the center of gravity of level E_2 shows a positive shift. This means that the population of level E_3 will not only depopulate level E_2 and weaken its dipole, but it will also induce a dipole between E_2 and E_3 which goes into the opposite direction of the dipole between levels E_1 and E_2. There are therefore two simultaneous effects which will induce a weakening of the total photovoltaic signal. Comparing the absorption probabilities of the different processes results in a quadratic saturation effect, as experimentally observed.

6. High frequency testing

After having seen that the electronic lifetime in a GaN QW can be as short as 170 fs, and given the fact that intersubband transitions are possible down to 1.4 μm, it was very appealing to investigate the high frequency performance of the detectors. For this purpose, we used a diode laser beam at 1.55 μm which

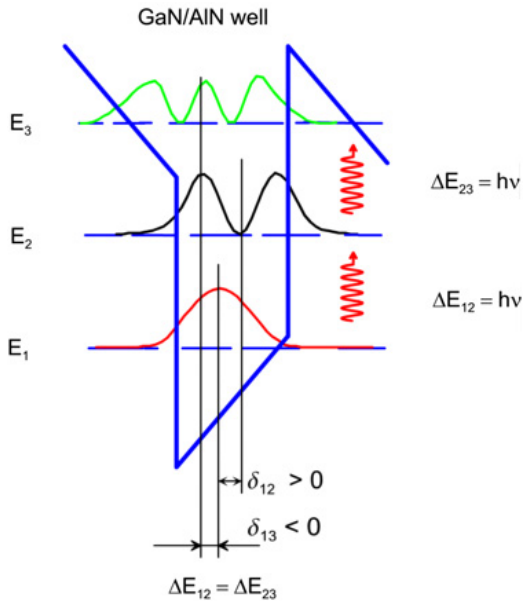

Figure 16. Schematic drawing of an AlN/GaN QW with the wavefunctions of its first three bound states. The different directions of the displacements for the levels are clearly visible.

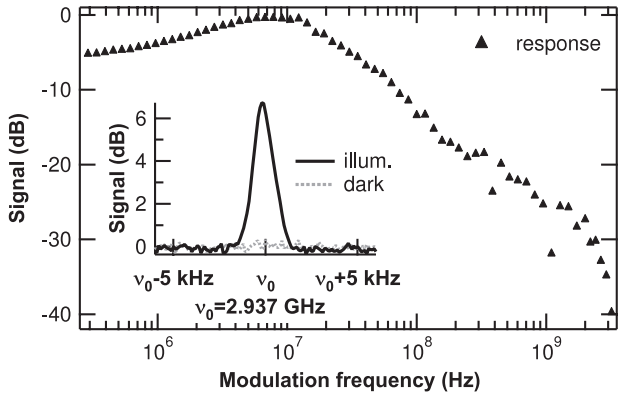

Figure 17. Typical detector signal versus measurement frequency plot for an AlN/GaN-based intersubband detector working at 1.55 μm. A maximum frequency of 3 GHz was achieved in this experiment.

was modulated via a commercial electro-optical modulator having an extinction ratio of >10 dB. The laser delivered 20 mW output power. In order to reduce electrical cross-talk problems, we physically separated the laser with its modulator equipment from the detector and its amplifier. A 30 m long single mode fiber connected the laser and detector parts of the experiment. Amplification of the detector signal was in this case done with a Sonoma 317 amplifier which reached its 3 dB point at 2.5 GHz. A typical characterization curve is shown in figure 17. It shows the amplified detector signal as a function of measurement frequency up to 3 GHz. The maximum signal was seen at 40 MHz, while a -20 dB/decade slope could be observed up to about 2 GHz. From then on, the slope became twice as steep. This is shown even more clearly in figure 18, where a different measurement technique has been used. In this experiment, we took ultra-short pulsed

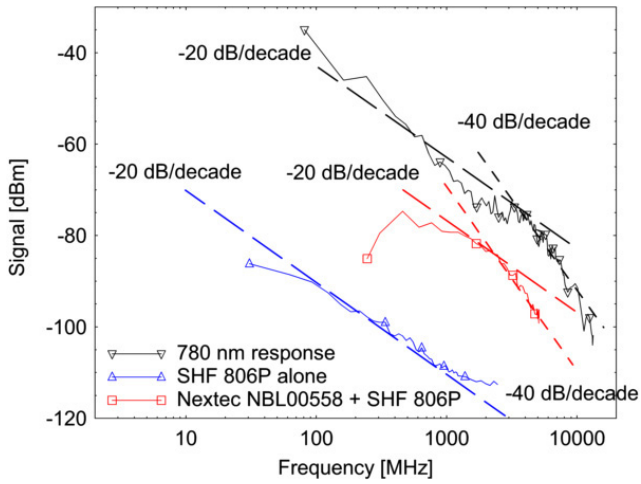

Figure 18. Testing of the detector's maximal frequency range using an ultra-short pulse solid state laser source.

solid state lasers with pulse durations of the order of 200 fs and a pulse repetition frequency of 30 MHz (Yb-doped fiber laser, 1550 nm) to 81 MHz (Nd:YAG laser, 780 nm). Looking at the Fourier transform of the measured pulse shape allowed us then to directly determine the frequency response of the detector, at least as long as we stayed sufficiently far from the inverse of the pulse length. This was always the case since our measurements did not exceed 15 GHz. As shown in figure 18, we measured a maximum frequency of 5 GHz for the $E_1 \rightarrow E_2$ transition, and of 13.3 GHz for the $E_1 \rightarrow E_3$ transition [69]. As an interesting detail, we observed the change in steepness at the same frequency for both measurement wavelengths, namely at roughly 2.2 GHz. This frequency is therefore a device- or mounting-intrinsic property and is most likely due to the relatively long (6.5 mm, diameter 25 μm) bond wire which connects the detector active surface to the central pin of the BNC connector. Future experiments should take care to make this connection as short as possible, as demonstrated in Hofstetter *et al* [70, 71].

7. Quantum cascade detectors and quantum dot infrared photodetectors

The present manuscript would not be complete without a short description of other types of AlN/GaN-based infrared detectors. Very recently, a quantum cascade detector (QCD) was presented by Vardi *et al* [72]. Like its mid-infrared counterparts, this device also profits from a photovoltaic mode of operation. The band structure is engineered in such a way as to vertically transport excited electrons by means of a built-in potential ramp. In order to fabricate such a device, the use of both binary and ternary compounds, namely AlN, GaN, and AlGaN, was necessary. A schematic band structure is shown in figure 19, and the photovoltaic response of the device to near-infrared radiation is presented in figure 20. In contrast to an AlN/GaN superlattice photodetector based on an optical rectification process as described above, a QCD can potentially reach a higher responsivity. In the example shown

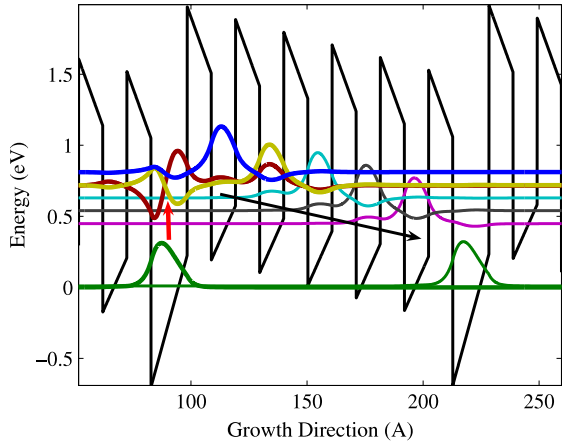

Figure 19. Schematic band structure of a near-infrared QCD. The transport direction is given by the slope of the potential ramp.

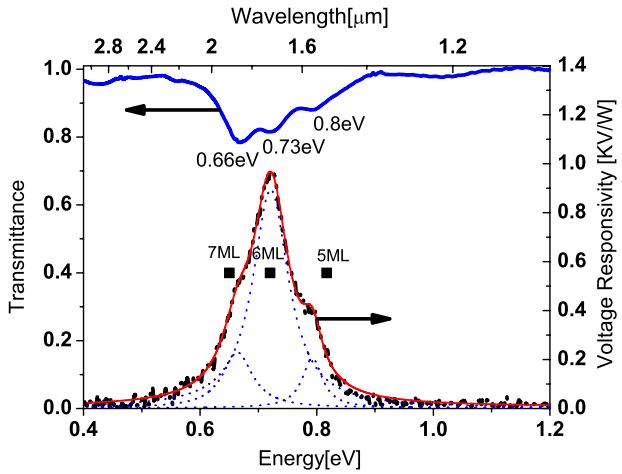

Figure 20. Spectral responsivity of the QCD represented schematically in the previous graph.

in figure 20, a voltage responsivity of 1 kV W^{-1} was seen in photovoltaic mode of operation. Using an internal device resistance of 100 kΩ, a current responsivity of 10 mA W^{-1} can be calculated for this first demonstrator. As a comparison, only 0.1 mA W^{-1} were demonstrated in the first GaN/AlN-based QW detector. This difference is mainly due to the fact that in a QCD, electrons are being physically transported across the entire structure and not only displaced by a couple of angstroms. In addition, the QCD also offers a higher degree of design freedom which will eventually allow broader wavelength coverage.

As a second example of an alternative III-nitride-based photodetector, we would like to mention the quantum dot infrared photodetector (QDIP). Such a device was first demonstrated in 2006 by Vardi *et al* [73]. Its wavelength characteristics are similar to the QW-based devices described in the present article. Its potential advantage is clearly that it can absorb not only TM-, but also transverse electrical (TE)-polarized light, which facilitates optical coupling into the device. Another interesting property is the fact that this photodetector works well in photoconductive mode, which results in photoconductive gain. Indeed, a room temperature responsivity of the order of 8 mA W^{-1} has been observed for this device.

8. Conclusions

In conclusion, we have reviewed recent progress in growth, fabrication, testing, and theoretical understanding of AlN/GaN-based intersubband detectors for the mid-infrared wavelength range. It is now clear that such devices can work at frequencies up to tens of GHz, show interesting non-linear effects, and are capable of integration with transistors or ultraviolet detectors [74]. The work has also shown, however, that the III-nitrides still suffer from a certain lack of knowledge in terms of fundamental material parameters. We therefore believe that future work on this topic will potentially have a high pay-off not only for ultra-fast telecommunication systems, but also for applications in laser and light emitting diode technology, especially regarding defect levels and their interaction with light.

Acknowledgments

The authors would like to thank the Professorship Program and the National Center of Competence in Research, both sponsored from the Swiss National Science Foundation, the US Office of Naval Research under grant N00014-08-1-4005 monitored by Dr David Marquis, the European Commission under contract NitWave (No. 004170), and ArmaSuisse for their generous financial support. AlN-on-sapphire templates were provided by DOWA Electronics Materials Inc.

References

[1] Ando T, Fowler A B and Stern F 1982 Electronic properties of two-diemnsional electronic systems *Rev. Mod. Phys.* **54** 437
[2] West L C and Eglash S J 1985 First observation of an extremely large-dipole infrared transition within the conduction band of a GaAs quantum well *Appl. Phys. Lett.* **46** 1156
[3] Levine B F, Choi K K, Bethea C G, Walker J and Malik R J 1987 New 10 μm infrared detector using intersubband absorption in resonant tunneling GaAlAs superlattices *Appl. Phys. Lett.* **50** 1092
[4] Choi K-K, Levine B F, Bethea C G, Walker J and Malik R J 1987 Multiple quantum well 10 μm GaAs/$Al_xGa_{1-x}As$ infrared detector with improved responsivity *Appl. Phys. Lett.* **50** 1814
[5] Liu H C, Li Jianmeng, Brown E R, McIntosh K A, Nichols K B and Manfra M J 1995 Quantum well intersubband heterodyne infrared detection up to 82 GHz *Appl. Phys. Lett.* **67** 1594
[6] Faist J, Capasso F, Sivco D L, Sirtori C, Hutchinson A L and Cho A Y 1994 Quantum cascade laser *Science* **264** 553–6
[7] Beck M, Hofstetter D, Aellen T, Faist J, Oesterle U, Ilegems M, Gini E and Melchior H 2002 Continuous wave operation of a mid-infrared semiconductor laser at room temperature *Science* **295** 301–5
[8] Bai Y, Darvish S R, Slivken S, Zhang W, Evans A, Nguyen J and Razeghi M 2008 Room temperature continuous wave operation of quantum cascade lasers with watt-level optical power *Appl. Phys. Lett.* **92** 101105

[9] Rochat M, Ajili L, Willenberg H, Faist J, Beere H, Davies G, Linfield E and Ritchie D 2002 Low-threshold terahertz quantum-cascade lasers *Appl. Phys. Lett.* **81** 1381

[10] Walther C, Fischer M, Scalari G, Terazzi R, Hoyler N and Faist J 2007 Quantum cascade lasers operating from 1.2 to 1.6 THz *Appl. Phys. Lett.* **91** 131122

[11] Gopal A V, Yoshida H, Neogi A, Georgiev N, Mozume T, Simoyama T, Wada O and Ishikawa H 2002 Intersubband absorption saturation in InGaAs–AlAsSb quantum wells *IEEE J. Quantum Electron.* **38** 1515

[12] Akimoto R, Li B S, Akita K and Hasama T 2005 Subpicosecond saturation of intersubband absorption in (CdS/ZnSe)/BeTe quantum-well waveguides at telecommunication wavelength *Appl. Phys. Lett.* **87** 181104

[13] Ma B S *et al* 2007 GaInNAs double-barrier quantum well infrared photodetector with the photodetection at 1.24 μm *Appl. Phys. Lett.* **91** 051102

[14] Gmachl C, Ng H M, Chu S N G and Cho A Y 2000 Intersubband absorption at $\lambda \sim 1.55$ μm in well- and modulation-doped GaN/AlGaN multiple quantum wells with superlattice barriers *Appl. Phys. Lett.* **77** 3722

[15] Gmachl C, Ng H M and Cho A Y 2001 Intersubband absorption in degenerately doped GaN/$Al_xGa_{1-x}N$ coupled double quantum wells *Appl. Phys. Lett.* **79** 1590

[16] Kishino K, Kikuchi A, Kanazava H and Tachibana T 2002 Intersubband transition in (GaN)(m)/(AlN)(n) superlattices in the wavelength range from 1.08 to 1.61 μm *Appl. Phys. Lett.* **81** 1234

[17] Helman A *et al* 2003 Intersubband spectroscopy of doped and undoped GaN/AlN quantum wells grown by molecular-beam epitaxy *Appl. Phys. Lett.* **83** 5196

[18] Suzuki N and Iizuka N 1999 Effect of polarization field on intersubband transition in AlGaN/GaN quantum wells *Japan. J. Appl. Phys.* **38** L363

[19] Nicolay S, Carlin J F, Feltin E, Butte R, Mosca M, Grandjean N, Ilegems M, Tchernycheva M, Nevou L and Julien F H 2005 Midinfrared intersubband absorption in lattice-matched AlInN/GaN multiple quantum wells *Appl. Phys. Lett.* **87** 111106

[20] Tchernycheva M, Nevou L, Doyennette L, Julien F H, Warde E, Guillot F, Monroy E, Bellet-Amalric E, Remmele T and Albrecht M 2006 Systematic experimental and theoretical investigation of intersubband absorption in GaN/AlN quantum wells *Phys. Rev.* B **73** 125347

[21] Cywiński G *et al* 2006 Growth of thin AllnN/GalnN quantum wells for applications to high-speed intersubband devices at telecommunication wavelengths *J. Vac. Sci. Technol.* B **24** 1505

[22] Martin G, Strite S, Botchkarev A, Agarwal A, Rockett A, Lambrecht W R L, Segall B and Morkoç H 1995 Valence band discontinuity between GaN and AlN measured by x-ray photoemission spectroscopy *J. Electron. Mater.* **225** 24

[23] Wei S and Zunger A 1996 Valence band splittings and band offsets of AlN, GaN, and InN *Appl. Phys. Lett.* **69** 2719

[24] Martin G, Botchkarev A, Rockett A and Morkoç H 1996 Valence-band discontinuities of wurtzite GaN, AlN, and InN heterojunctions measured by x-ray photoemission spectroscopy *Appl. Phys. Lett.* **68** 2541

[25] Iizuka N, Kaneko K, Suzuki N, Asano T, Noda S and Wada O 2000 Ultrafast intersubband relaxation ($\leqslant$150 fs) in AlGaN/GaN multiple quantum wells *Appl. Phys. Lett.* **77** 648

[26] Wang Z, Reimann K, Woerner M, Elsaesser T, Hofstetter D, Hwang J, Schaff W J and Eastman L F 2004 Femtosecond intersubband dynamics of electrons in AlGaN/GaN-based high-electron-mobility transistors *Semicond. Sci. Technol.* **19** S463–4

[27] Gmachl C, Ng H M and Cho A Y 2000 Intersubband absorption in GaN/AlGaN multiple quantum wells in the wavelength range of $\lambda \sim 1.75$–4.2 μm *Appl. Phys. Lett.* **77** 334

[28] Wang Z, Reimann K, Woerner M, Elsaesser T, Hofstetter D, Baumann E, Giorgetta F R, Wu H, Schaff W J and Eastman L F 2006 Ultra-fast hole-burning in intersubband absorption lines of GaN/AlN superlattices *Appl. Phys. Lett.* **89** 151103

[29] Heber J D, Gmachl C, Ng H M and Cho A Y 2002 Comparative study of ultrafast intersubband electron scattering times at $\sim$1.55 μm wavelength in GaN/AlGaN heterostructures *Appl. Phys. Lett.* **81** 1237

[30] Asano T, Yoshizawa S, Noda S, Iizuka N, Kaneko K, Suzuki N and Wada O 2001 Ultrafast all optical modulation based on intersubband transition in semiconductor quantum wells *Opt. Quantum Electron.* **33** 963–73

[31] Hofstetter D, Faist J and Bour D P 2000 Mid-infrared emission from InGaN/GaN-based light emitting diodes *Appl. Phys. Lett.* **76** 1495–7

[32] Tchernycheva M, Nevou L, Doyennette L, Helman A, Colombelli R, Julien F H, Guillot F, Monroy E, Shibata T and Tanaka M 2005 Intraband absorption of doped GaN/AlN quantum dots at telecommunication wavelengths *Appl. Phys. Lett.* **87** 101912

[33] Hofstetter D, Schad S-S, Wu H, Schaff W J and Eastman L F 2003 GaN/AlN-based quantum well infrared photodetector for 1.55 μm *Appl. Phys. Lett.* **83** 572–4

[34] Lupu A *et al* 2008 Lattice-matched GaN/InAlN waveguides at 1.55 μm grown by metalorganic vapor phase epitaxy *IEEE Photon. Technol. Lett.* **20** 102–4

[35] Vardi A, Akopian N, Bahir G, Doyennette L, Tchernycheva M, Nevou L, Julien F H, Guillot F and Monroy E 2006 Room temperature demonstration of GaN/AlN quantum dot intraband infrared photodetector at fiber-optics communication wavelength *Appl. Phys. Lett.* **88** 143101

[36] Baumann E, Giorgetta F R, Hofstetter D, Wu H, Schaff W J, Eastman L F and Kirste L 2005 Tunnelling effects and intersubband absorption in AlN/GaN superlattices *Appl. Phys. Lett.* **86** 032110–2

[37] Wang Z, Reimann K, Woerner M, Elsaesser T, Hofstetter D, Hwang J, Schaff W J and Eastman L F 2005 Optical phonon sidebands of electronic intersubband absorption in strongly polar semiconductors *Phys. Rev. Lett.* **94** 037403–6

[38] Baumann E, Giorgetta F R, Hofstetter D, Guillot F, Bellet-Amalric E and Monroy E 2006 Tunable electro-modulated intersubband absorption of a GaN/AlN superlattice grown on a transistor-like structure *Appl. Phys. Lett.* **89** 101121

[39] Baumann E, Giorgetta F R, Hofstetter D, Guillot F, Leconte S, Bellet-Amalric E and Monroy E 2007 GaN/AlN electro-optical modulator prototype at telecommunication wavelengths *Phys. Status Solidi* c **4** 1621–4

[40] Baumann E, Giorgetta F R, Hofstetter D, Golka S, Schrenk W, Strasser G, Kirste L, Nicolay S, Feltin E and Grandjean N 2006 1.5 μm absorption and room temperature photovoltaic response in AlN/GaN superlattices grown by metalorganic vapor phase epitaxy *Appl. Phys. Lett.* **89** 041106

[41] Baumann E, Giorgetta F R, Hofstetter D, Lu H, Chen X, Schaff W J, Eastman L F, Golka S, Schrenk W and Strasser G 2005 Intersubband photoconductivity at 1.6 μm using a strain-compensated AlN/GaN superlattice *Appl. Phys. Lett.* **87** 191102–4

[42] Nevou L, Tchernycheva M, Julien F H, Guillot F and Monroy E 2007 *Appl. Phys. Lett.* **90** 121106

[43] Hofstetter D, Baumann E, Giorgetta F R, Graf M, Maier M, Guillot F, Bellet-Amalric E and Monroy E 2006 High-quality AlN/GaN-superlattice structures for the fabrication of narrow-band 1.4 μm photovoltaic intersubband detectors *Appl. Phys. Lett.* **88** 121112

[44] Giorgetta F R, Baumann E, Guillot F, Monroy E and Hofstetter D 2007 High frequency ($f = 2.37$ GHz) room

temperature operation of 1.55 μm AlN/GaN-based intersubband detector *Electron. Lett.* **43** 185–7
[45] Hofstetter D, Baumann E, Giorgetta F R, Guillot F, Leconte S and Monroy E 2007 Optically non-linear effects in intersubband transitions of GaN/AlN-based superlattices *Appl. Phys. Lett.* **91** 131115
[46] Kheirodin N *et al* 2008 Electrooptical modulator at telecommunication wavelengths based on GaN-AIN coupled quantum wells *IEEE Photon. Technol. Lett.* **20** 724–6
[47] Suzuki N 2003 Simulation of ultrafast cross-gain modulation in optically-pumped GaN/AlN intersubband optical amplifiers *Japan. J. Appl. Phys.* **42** 5607–12
[48] Iizuka N, Kaneko K and Suzuki N 2000 Sub-picosecond all-optical gate utilizing aN intersubband transition *Opt. Express* **13** 3835–40
[49] Iizuka N, Kaneko K and Suzuki N 2002 Near-infrared intersubband absorption in GaN/AlN quantum wells grown by molecular beam epitaxy *Appl. Phys. Lett.* **81** 1803
[50] Iizuka N, Kaneko K and Suzuki N 2004 Sub-picosecond modulation by intersubband transition in ridge waveguide with GaN/AIN quantum wells *Electron. Lett.* **40** 962
[51] Iizuka N, Kaneko K and Suzuki N 2006 Polarization dependent loss in III-nitride optical waveguides for telecommunication devices *J. Appl. Phys.* **99** 093107
[52] Li Y, Bhattacharyya A, Thomidis C, Moustakas T D and Paiella R 2007 Ultrafast all-optical switching with low saturation energy via intersubband transitions in GaN/AlN quantum-well waveguides *Opt. Express* **15** 17922
[53] Tyagai V A, Evstigneev A M, Krasiko A N, Andreeva A F and Malakhov V Y 1977 Optical properties of indium nitride films *Sov. Phys.—Semicond.* **11** 1257
[54] Wu J, Walukiewicz W, Yu K M, Ager J W III, Haller E E, Lu H, Schaff W J, Saito Y and Nanishi Y 2001 Unusual properties of the fundamental bandgap of InN *Appl. Phys. Lett.* **80** 3967
[55] Ambacher O *et al* 1999 Two-dimensional electron gases induced by spontaneous and piezoelectric polarization charges in N- and Ga-face AlGaN/GaN heterostructures *J. Appl. Phys.* **85** 3222
[56] Dimitrov R, Murphy M, Smart J, Schaff W J, Shealy J R, Eastman L F, Ambacher O and Stutzmann M 2000 Two-dimensional electron gases in Ga-face and N-face AlGaN/GaN heterostructures grown by plasma-induced molecular beam epitaxy and metalorganic chemical vapor deposition on sapphire *J. Appl. Phys.* **87** 3375
[57] Foisy M C 1990 A physical model for the bias dependence of the modulation-doped field-effect transistor's high frequency performance *PhD Thesis* Cornell University
[58] Foisy M C, Tasker P J, Hughes B and Eastman L F 1988 The role of inefficient charge modulation in limiting the current-gain cutoff frequency of the MODFET *IEEE Trans. Electron Devices* **35** 871–8
[59] Sirtori C, Capasso F, Faist J and Scandolo S 1994 Nonparabolicity and a sum rule associated with bound-to-bound and bound-to-continuum intersubband transitions in quantum wells *Phys. Rev.* B **50** 8663–74
[60] Ambacher O *et al* 2002 Pyroelectric properties of Al(In)GaN/GaN hetero- and quantum well structures *J. Phys.: Condens. Matter* **34** 3399–434
[61] Bernardini F, Fiorentini V and Vanderbilt D 2002 Spontaneous polarization and piezoelectric constants of III–V nitrides *Phys. Rev.* B **56** 10024–7
[62] Monroy E, Andreev T, Holliger P, Bellet-Amalric E, Shibata T, Tanaka M and Daudin B 2004 Modification of GaN(0001) growth kinetics by Mg-doping *Appl. Phys. Lett.* **84** 2554
[63] Rosa A L, Neugebauer J, Northrup J E, Lee C-D and Feenstra R M 2002 Adsorption and incorporation of Si at GaN(0001) surfaces *Appl. Phys. Lett.* **80** 2008
[64] Monroy E, Guillot F, Gayral B, Bellet-Amalric E, Jalabert D, Gérard J-M, Dang Le Si, Tchernycheva M and Julien F H 2006 Observation of hot luminescence and slow inter-sub-band relaxation in Si-doped GaN/$Al_xGa_{1-x}N$ ($x = 0.11, 0.25$) multi-quantum-well structures *J. Appl. Phys.* **99** 093513
[65] Monroy E, Daudin B, Bellet-Amalric E, Gogneau N, Jalabert D, Enjalbert F, Brault J, Barjon J and Dang Le Si 2003 Surfactant effect of In for AlGaN growth by plasma-assisted molecular beam epitaxy *J. Appl. Phys.* **93** 1550
[66] Tchernycheva M, Nevou L, Doyennette L, Collombelli R, Julien F H, Guillot F, Monroy E, Bellet-Amalric E, Remmele T and Albrecht M 2006 *Phys. Rev.* B **73** 125347
[67] Rosencher E, Bois Ph, Vinter B, Nagle J and Kaplan D 1990 *Appl. Phys. Lett.* **56** 1822
[68] Rosencher E and Bois Ph 1991 *Phys. Rev.* B **44** 11315
[69] Hofstetter D, Baumann E, Giorgetta F R, Dawlaty J, George P A, Rana F, Guillot F and Monroy E 2008 High frequency measurements on an AlN/GaN-based intersubband detector at 1550 and 780 nm *Appl. Phys. Lett.* **92** 231104
[70] Graf M, Scalari G, Hofstetter D, Faist J, Beere H, Davies G, Linfield E and Ritchie D 2004 AlGaAs-based THz range quantum well infrared photodetector at 87 μm *Appl. Phys. Lett.* **84** 475–7
[71] Hofstetter D, Graf M, Aellen T, Faist J, Hvozdara L and Blaser S 2006 23 GHz operation of a room temperature photovoltaic quantum cascade detector at 5.35 μm *Appl. Phys. Lett.* **89** 061119
[72] Vardi A, Bahir G, Guillot F, Bougerol C, Monroy E, Schacham S E, Tchernycheva M and Julien F H 2008 Near-infared quantum cascade detector in GaN/AlGaN/AlN heterostructures *Appl. Phys. Lett.* **92** 011112
[73] Vardi A, Akopian N, Bahir G, Doyennette L, Tchernycheva M, Nevou L, Julien F H, Guillot F and Monroy E 2006 Room temperature demonstration of GaN/AlN quantum dot intraband infrared photodetector at fiber-optics communication wavelength *Appl. Phys. Lett.* **88** 143101
[74] Hofstetter D, Theron R, Baumann E, Giorgetta F R, Golka S, Strasser G, Guillot F and Monroy E 2008 Monolithically integrated AlGaN/GaN/AlN-based solar-blind ultraviolet and near-infrared detectors *Electron. Lett.* **44** 986–8